Energy-Efficient M-QAM Precoder Design with Spatial Peak Power Minimization for MIMO Directional Modulation Transceivers

Ashkan Kalantari, Christos Tsinos, Mojtaba Soltanalian,
Symeon Chatzinotas, Wing-Kin Ma, and Björn Ottersten

arXiv:1702.06878v1 [cs.IT] 22 Feb 2017

***Abstract*—Spectrally efficient multi-antenna wireless communications is a key challenge as service demands continue to increase. At the same time, powering up radio access networks increases CO_2 footprint. Hence, for an efficient radio access design, we design a directional modulation precoder for M-QAM modulation with $M = 4, 8, 16, 32$. First, extended detection regions are defined in these constellations using analytical geometry. Then, constellation points are placed in the optimal positions of these regions while the minimum Euclidean distance to neighbor constellation points and detection region boundary is kept as in the conventional M-QAM modulation. For further energy-efficiency, relaxed detection regions are modeled for inner points of $M = 16, 32$ constellations. The modeled extended and relaxed detection regions as well as the modulation characteristics are utilized to formulate convex symbol-level precoder design problems for directional modulation to minimize the transmission power while preserving the minimum required SNR at the destination. In addition, the extended and relaxed detection regions are used for precoder design to minimize the output of each power amplifier. Results show that compared to the benchmark schemes, the proposed methods perform better in terms of power and peak power reduction as well as symbol error rate reduction for a long range of SNRs.**

***Keywords*—Directional modulation, energy efficiency, extended detection region, spatial peak power, M-QAM modulation, symbol-level precoding.**

I. Introduction

According to Cisco's prediction [1], mobile data traffic, primarily driven by video demand, will increase eleven-fold from 2015 to 2020. The extreme growth of video content on the Internet, the advent of mobile devices, e.g., smart phones and tablets, and the market appetite for them are the most important elements which have contributed to the tremendous surge in mobile traffic. Conventional approaches such as orthogonal frequency division multiplexing access and time division multiplexing access [2], [3] are used to utilize the frequency and time resources in order to improve the data communication rate. To use the spatial dimension, Multiple-input Multiple-output (MIMO) communication systems emerged, e.g., Long Term Evolution (LTE) and WiFi technologies. MIMO systems provide spatial degree of freedom in the design at the expense of interference among the transmitted data streams. In order to better utilize the available degrees of freedom, pre/post-processing at the transmitter and/or receiver ends are employed [4], [5] to reduce the interference among the data streams. Recently, there has been a growing interest in directional modulation [6]–[11] and symbol-level precoding for constructive interference [12]–[15] techniques to mitigate interference in MIMO communication systems. In directional modulation, the channel realization and the symbols are used to design the the antenna weights. These weights are designed such that the Radio Frequency (RF) signals get modulated after passing through the channel and result in communicating the desired symbol at the desired direction (antenna). Depending on the design, this can result in no interference [9], [11] or limited interference [7], [10] among the communicated data streams. Both digital symbol-level precoding and directional modulation focus on multiplexing gain in MIMO communication systems. Directional modulation and digital symbol-level precoding for constructive interference differ in the following way. The former focuses on applying array weights in the analog domain to have the desired amplitude and phase for the received signals, while the latter uses symbol-level precoding for digital signal design at the transmitter to create constructive interference at the receiver.

Apart from an increasing data demand, wireless communications consume a large amount of energy and have a considerable share in environmental pollution [16]. Not only reducing the energy consumed in the radio access networks is environmental friendly, but it also decreases the communication costs for both the operators and users [17]. The research works in [9], [12], [13], [18], [19] study the relaxed design in constructive interference and directional modulation with the goal of reducing the energy consumption at the transmitter.

Although directional modulation offers transmission with no or limited interference as well as energy-efficiency, the hardware limitations at the transmitter need to be considered in the precoder design process. Among the hardware limitations, we focus on keeping the power amplifier outside its saturation region. In the architecture of a directional modulation transmitter, the RF oscillator signal is equally divided among the RF chains [6]–[9]. Each power amplifier needs to operate within

This work was supported by the National Research Fund (FNR) of Luxembourg under AFR grant for the project SeMIGod. Ashkan Kalantari, Christos Tsinos, Symeon Chatzinotas, and Björn Ottersten are with the Interdisciplinary Centre for Security, Reliability and Trust (SnT), The University of Luxembourg, 29, avenue JF Kennedy, L-1855 Luxembourg-Kirchberg, Luxembourg, (E-mails: {ashkan.kalantari,christos.tsinos,symeon.chatzinotas,bjorn.ottersten}@uni.lu). Mojtaba Soltanalian is with the Department of Electrical and Computer Engineering, University of Illinois at Chicago, Chicago, IL 60607, E-mail: (msol@uic.edu). Wing-Kin Ma is with the Department of Electronic Engineering, The Chinese University of Hong Kong, Shatin, Hong Kong, China (e-mail:wkma@ieee.org).

a specific range to avoid nonlinear distortion of the amplified signal [20]. To avoid distortion in the amplified signal, we need to design the antenna weights such that the output of each power amplifier does not go into the saturation region. In this direction, the references [21], [22] consider constant envelope precoding for a single-user massive MIMO system. However, the design condition of a constant envelop design is restrictive and results in a conservative design. The authors in [23] consider a low peak power to average ratio design based on constructive interference for M-PSK modulation to limit the amplifier output power below a specific value where there is a strict constraint on the phase of the received symbols. A relaxed low peak power design for M-PSK modulation in order to include both energy efficiency and hardware limitation is proposed in [10].

A. Contributions and Main Results

Based on the above descriptions, we tackle the design of a system which jointly takes into account the user demand, power amplifier saturation as a hardware limitation, and energy efficiency when finite-alphabet input is considered. The designed precoders for Gaussian input signals can be used to precode finite-alphabet inputs, however, this may result in considerable system performance reduction [24].

The works of [9], [10], [12], [13], [18], [19] focus on M-PSK precoder design. However, there is no work on designing the M-QAM directional modulation precoder for $M = 4, 8, 16, 32$, while jointly utilizing the extended and relaxed detection regions of the constellation as well as controlling the power of the amplifier output signal to avoid saturation. To pursuit this design, we use the concept of directional modulation to jointly address the data rate and energy-efficiency issues of wireless communications while considering the limit on power amplifier outputs. In the directional modulation, instead of producing the symbols at the transmitter and sending them, the channel state information and the symbols to be communicated are used to produce the phase and amplitude of each transmitter RF chain. Then, the transmitted RF signals are modulated after passing through the channel and create the required symbols on the intended antennas. Depending on the design, directional modulation can induce exact symbols, which can be translated into the interference-free communication, or induce a close value (amplitude and phase) to the symbols, which can be translated into communication with interference, on the receiving antennas.

In this paper, we bring the following contributions:

1) We define the extended detection regions of M-QAM modulation for $M = 4, 8, 16, 32$ and model these regions using analytical geometry. By extended detection region, we mean a region in which a constellation point can be placed, given that it preserves the standard distance with the neighbor constellation points and the detection boundaries. Here, the Euclidean distance among the constellation points in conventional M-QAM is considered as the standard distance. The work of [15] considers symbol-level precoder design for $M = 16$.
2) In addition to the extended detection regions, we characterize relaxed detection regions where the inner points of $M = 16, 32$ constellations can be placed in a region rather than being fixed. Using the extended detection region, we can setup a trade-off between further energy-efficiency at the transmitter and symbol error rate (SER) at the receiver. The research [11] performs directional modulation precoder design for $M = 4, 8, 16, 32$ constellations by only using extended detection region without considering peak power minimization. The work of [15] does not design the precoder when relaxed detection region is considered for inner point of $M = 16$ constellations.
3) We design the optimal M-QAM directional modulation precoder using the characterized extended detection regions for $M = 4, 8, 16, 32$ to minimize the transmission power while satisfying the required SNR at the antennas of the receiver. Furthermore, we re-design the optimal precoder for $M = 16, 32$ constellations while considering the relaxed detection region for inner constellation points in addition to the extended detection regions for outer constellation points and investigate the energy-efficiency and SER.
4) We design the optimal precoder to minimize the instantaneous peak power of the amplifier output signal for each RF chain of the directional modulation transmitter. We refer to this as spatial peak power minimization defined as

$$P_{\max}^{spatial} = \max_{k=1,\ldots,N_t} \mathbf{w}^H \mathbf{E}_k \mathbf{w}. \tag{1}$$

   We carry out this design using the characterized extended detection regions for $M = 4, 8, 16, 32$ while preserving the required SNR at the antennas of the receiver. Also, we repeat the precoder design while considering both relaxed and extended detection regions for $M = 16, 32$. In [23], the spatial peak power minimization is carried out for M-PSK modulation without considering extended and relaxed detection regions.
5) Through extensive simulations, we reveal the benefits of using extended detection regions for M-QAM directional modulation transmission in terms of power reduction at the transmitter and SER improvement at the receiver. As a hardware limitation, we evaluate the performance in terms of the mentioned metrics when minimizing the instantaneous spatial peak power. In addition, we quantify the trade-off between power consumption and SER when relaxed detection regions are used while this is not investigated in [15].

The design for $M = 4, 8$ translates into interference-free communication since the symbols keep the standard Euclidean distance. In addition, the precoder design when considering fixed inner constellation points for $M = 16, 32$ translates into the interference-free communication. On the other hand, the precoder design when considering relaxed inner constellation points for $M = 16, 32$ translates into the communication with interference.

It is worth mentioning that the precoder design for 128-QAM is similar to 32-QAM. Furthermore, the precoder design for 64-QAM and 256-QAM are similar to 16-QAM. Hence, we consider precoding design for $M = 4, 8, 16, 32$ constellation points in this work. From practical point of view, M-QAM modulations up to 64-QAM modulation are used in the long term evolution (LTE) standard [25].

B. Paper Organization

The remainder of this paper is organized as follows. In Section II, we introduce the signal and system model. The extended and relaxed detection regions are defined and modeled in Section III. In Section IV, the optimal M-QAM precoder design problems for total and spatial peak power minimization are formulated and transformed into standard convex forms. In Section V, we evaluate the proposed methods and compare them versus the benchmark scheme through simulations. At the end, we mention the conclusions in Section VI.

C. Notation

Upper-case and lower-case bold-faced letters are used to denote matrices and column vectors, respectively. The superscripts $(\cdot)^T$, $(\cdot)^*$, $(\cdot)^H$, and $(\cdot)^\dagger$ represent transpose, conjugate, Hermitian, and Moore-Penrose pseudo inverse operators, respectively. $\mathbf{I}_{N\times N}$ denotes an N by N identity matrix, $\mathbf{E}_k$ has one unit-valued element on the k-th diagonal entry with the rest of the elements being zero, $\widetilde{\mathbf{E}}_k$ has two unit-valued elements on the k-th and (N_t+k)-th diagonal entries with the rest of the elements being zero, $\mathrm{diag}(\mathbf{a})$ denotes a diagonal matrix where the elements of the vector $\mathbf{a}$ are its diagonal entries, $\mathbf{a}\circ\mathbf{b}$ is the element-wise Hadamard product, $\mathbf{0}$ is the all zero vector, $\|\cdot\|$ is the Frobenius norm, and $|\cdot|$ represents the absolute value of a scalar. $\mathrm{Re}\,(\cdot)$, $\mathrm{Im}\,(\cdot)$, and $\arg(\cdot)$ represent the real valued part, imaginary valued part, and angle of a complex number, respectively. $Card(\cdot)$ shows the number of set members.

II. Signal and System Model

Let us consider a directional modulation transmitter, denoted by T, having N_t antennas that communicates with a receiver, denoted by R, equipped by N_r antennas using M-QAM modulation where $M = 4, 8, 16, 32$. The received signal, $\mathbf{y}$, at R is

$$\mathbf{y} = \mathbf{H}\mathbf{w} + \mathbf{n}, \tag{2}$$

where $\mathbf{y}$ is an $N_r \times 1$ vector denoting the received signals by R, $\mathbf{H} = [\mathbf{h}_1, ..., \mathbf{h}_n, ..., \mathbf{h}_{N_r}]^T$ is an $N_r \times N_t$ matrix denoting the channel from T to R, $\mathbf{h}_n$ is an $N_t \times 1$ vector containing the channel coefficients from all the transmitter antennas to the n-th antenna of R, and $\mathbf{w}$ is the vector containing the weights of radio frequency (RF) chains which is the design variable in this work. The random variable $\mathbf{n} \sim \mathcal{CN}(\mathbf{0}, \sigma^2\mathbf{I}_{N_r\times N_r})$ denotes the additive white Gaussian noise at R, where $\mathcal{CN}$ denotes a complex and circularly symmetric random variable. The vector $\mathbf{s} = [s_1, ..., s_n, ..., s_{N_r}]$ contains the M-QAM symbols to be communicated between T and R using directional modulation technology, the elements of $\mathbf{H}\mathbf{w} = \left[s_1^{'}, ..., s_n^{'}, ..., s_{N_r}^{'}\right]^T$ are the induced M-QAM symbols on the antennas of R where $s_n^{'}$ is the induced M-QAM symbol on the n-th antenna of R. To detect the symbols, R can apply conventional detectors on each receiving antenna.

In this work, a single carrier is used to communicate symbols over a narrow band channel. Since the transmit precoder is designed such that the received signals have the desired amplitude and phase, a simple multiple-antenna receiver is considered which does not perform processing on the received signals.

In the next section, we characterize the extended and relaxed regions of the mentioned M-QAM constellations.

III. Characterization of Extended and Relaxed Detection Regions

In this part, we geometrically characterize the extended detection regions for $M = 4, 8, 16, 32$ constellations and relaxed detection regions for $M = 16, 32$ constellations. To do so, we derive analytical expressions which concisely describe these extended and relaxed detection regions. The extended detection regions are shown by solid areas and dashed lines in Fig. 1. As one can see, the extended detection region is an area in which the constellation point can be placed while keeping the distance to other constellations points more than or equal to the standard distance. Here, the Euclidean distance among the constellation points of conventional M-QAM modulation is considered as the standard distance. We divide each constellation into multiple sets, as illustrated in Figures 1(a) to 1(e), and continue to analytically model the extended and relaxed detection region of each set.

A. The Case of $M = 4$

Consider s_n as a symbol to be communicated with the n-th antenna of the receiver receiver. Considering that the received signal on the n-th antenna of the receiver is $\mathbf{h}_n^T\mathbf{w}$, the extended detection region for $s_n \in \mathfrak{s}_{\mathbf{1}_4}$ in the first quadrant of Fig. 1(a) can be modeled as

$$\begin{aligned} \mathrm{Re}\left(\mathbf{h}_n^T\mathbf{w}\right) &\geq \sqrt{\gamma}\mathrm{Re}\left(s_n\right), \\ \mathrm{Im}\left(\mathbf{h}_n^T\mathbf{w}\right) &\geq \sqrt{\gamma}\mathrm{Im}\left(s_n\right), \end{aligned} \tag{3}$$

where γ is the minimum required amplification for the induced symbol at the receiving antennas. The value of γ is derived from the required SNR value in dB at the receiver as $\gamma = 10^{SNR/10}$. The extended detection region defined in (3) cannot be used in other quadrants due to change in the sign of real and imaginary parts of s_n. However, we can multiply both sides of the equations by $\mathrm{Re}\left(s_n\right)$ and $\mathrm{Im}\left(s_n\right)$ to make both sides positive. Note that the direction of inequalities does not change since $\mathrm{Re}\left(s_n\right)$ and $\mathrm{Im}\left(s_n\right)$ have the same sign as $\mathrm{Re}\left(\mathbf{h}_n^T\mathbf{w}\right)$ and $\mathrm{Im}\left(\mathbf{h}_n^T\mathbf{w}\right)$, respectively, at the optimal point of precoder design. Hence, the extended detection region for any 4-QAM symbol, $s_n \in \mathfrak{s}_{\mathbf{1}_4}$, in Fig. 1(a) can be geometrically characterized using the following general expression:

$$\begin{aligned} \mathrm{Re}\left(s_n\right)\mathrm{Re}\left(\mathbf{h}_n^T\mathbf{w}\right) &\geq \sqrt{\gamma}\mathrm{Re}^2\left(s_n\right), \\ \mathrm{Im}\left(s_n\right)\mathrm{Im}\left(\mathbf{h}_n^T\mathbf{w}\right) &\geq \sqrt{\gamma}\mathrm{Im}^2\left(s_n\right). \end{aligned} \tag{4}$$

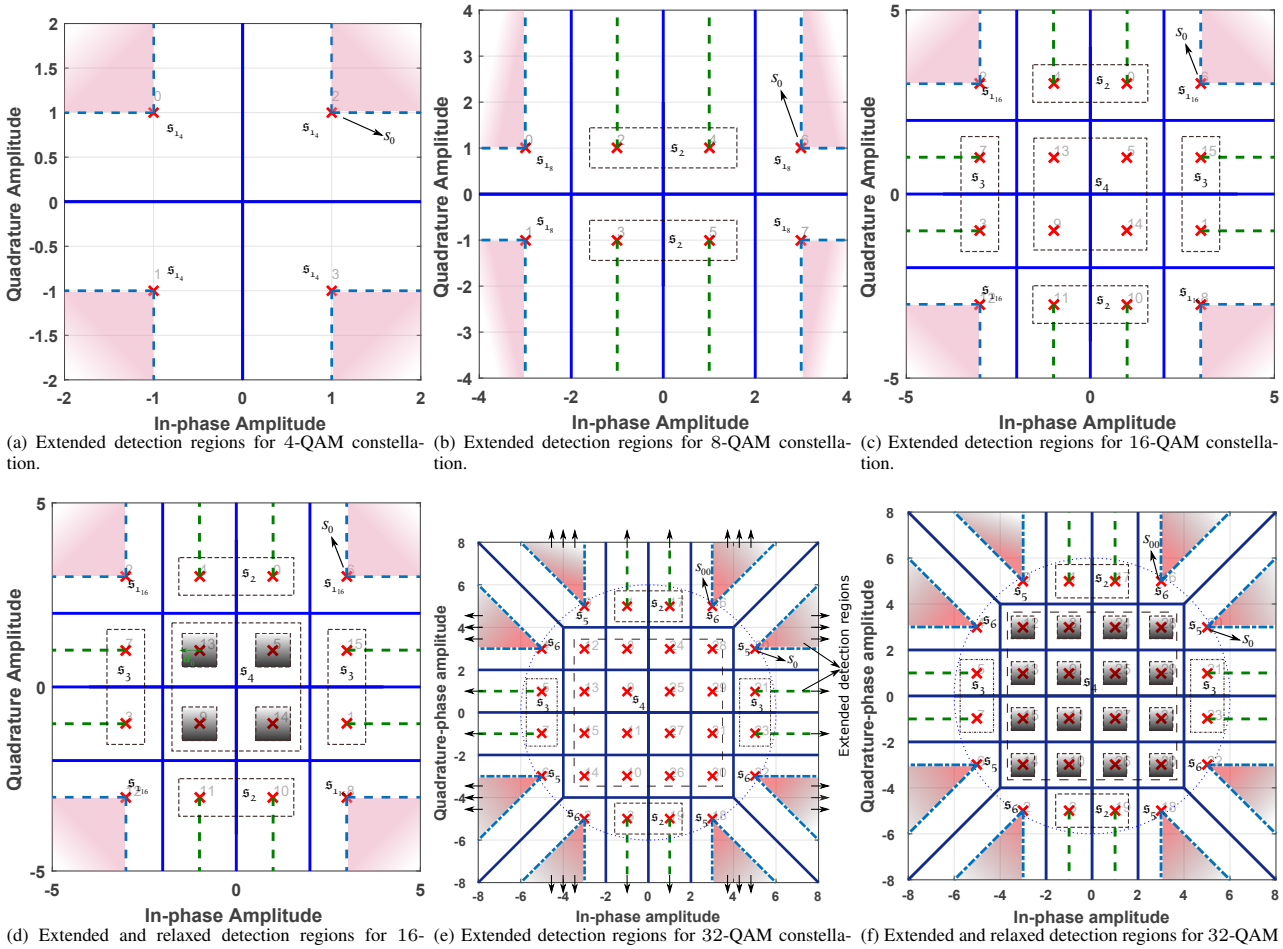

(a) Extended detection regions for 4-QAM constellation.
(b) Extended detection regions for 8-QAM constellation.
(c) Extended detection regions for 16-QAM constellation.
(d) Extended and relaxed detection regions for 16-QAM constellation.
(e) Extended detection regions for 32-QAM constellation.
(f) Extended and relaxed detection regions for 32-QAM constellation.

Fig. 1: Characterization of extended and relaxed detection regions for M-QAM constellations. The numbers show the decimal equivalent of the gray code for each symbol. The extended detection regions are shown by dashed lines and solid regions for $M = 4, 8, 16, 32$.

B. The Case of $M = 8$

The extended detection region of $s_n \in \mathfrak{s}_{1_8}$ for 8-QAM constellation in Fig. 1(b) can be characterized in the same way as (4). Next, the upper and lower sides of $s_n \in \mathfrak{s}_2$ can be characterized, respectively, as

$$\mathrm{Re}\left(\mathbf{h}_n^T\mathbf{w}\right) = \sqrt{\gamma}\mathrm{Re}\left(s_n\right),\ \mathrm{Im}\left(\mathbf{h}_n^T\mathbf{w}\right) \geq \sqrt{\gamma}\mathrm{Im}\left(s_n\right), \quad (5)$$

$$\mathrm{Re}\left(\mathbf{h}_n^T\mathbf{w}\right) = \sqrt{\gamma}\mathrm{Re}\left(s_n\right),\ \mathrm{Im}\left(\mathbf{h}_n^T\mathbf{w}\right) \leq \sqrt{\gamma}\mathrm{Im}\left(s_n\right). \quad (6)$$

The characterizations of $\mathfrak{s}_2$ in (5) and (6) can be fused to get a unified expression which describes the points in the set $\mathfrak{s}_2$ as

$$\begin{aligned}&\mathrm{Re}\left(\mathbf{h}_n^T\mathbf{w}\right) = \sqrt{\gamma}\mathrm{Re}\left(s_n\right),\\ &\mathrm{Im}\left(s_n\right)\mathrm{Im}\left(\mathbf{h}_n\mathbf{w}\right) \geq \sqrt{\gamma}\mathrm{Im}^2\left(s_n\right).\end{aligned} \quad (7)$$

C. The Case of $M = 16$

For $s_n \in \mathfrak{s}_{1_{16}}$ of 16-QAM constellation in Fig. 1(c), the extended detection region is characterized using (4). In addition, for $s_n \in \mathfrak{s}_2$ in Fig. 1(c), the characterization is the same as (7). The right-hand side and left-hand side extended detection regions of $s_n \in \mathfrak{s}_3$ can be characterized, respectively, as

$$\mathrm{Re}\left(\mathbf{h}_n^T\mathbf{w}\right) \geq \sqrt{\gamma}\mathrm{Re}\left(s_n\right),\ \mathrm{Im}\left(\mathbf{h}_n^T\mathbf{w}\right) = \sqrt{\gamma}\mathrm{Im}\left(s_n\right), \quad (8)$$

$$\mathrm{Re}\left(\mathbf{h}_n^T\mathbf{w}\right) \leq \sqrt{\gamma}\mathrm{Re}\left(s_n\right),\ \mathrm{Im}\left(\mathbf{h}_n^T\mathbf{w}\right) = \sqrt{\gamma}\mathrm{Im}\left(s_n\right), \quad (9)$$

which can be compressed into

$$\begin{aligned}&\mathrm{Re}\left(s_n\right)\mathrm{Re}\left(\mathbf{h}_n^T\mathbf{w}\right) \geq \sqrt{\gamma}\mathrm{Re}^2\left(s_n\right),\\ &\mathrm{Im}\left(\mathbf{h}_n^T\mathbf{w}\right) = \sqrt{\gamma}\mathrm{Im}\left(s_n\right).\end{aligned} \quad (10)$$

In the case $s_n \in \mathfrak{s}_4$, the points can be characterized in the following two ways.

1) Fixed detection region characterization for $s_n \in \mathfrak{s}_4$: In this approach, the points of $s_n \in \mathfrak{s}_4$ are considered in their own place. This satisfies the minimum standard distance between the constellation points and does not increase the SER compared to conventional 16-QAM. However, this modeling

does not improve the energy-efficiency. Accordingly, the constellation points $s_n \in \mathfrak{s}_4$ can be modeled as

$$\mathrm{Re}\left(\mathbf{h}_n^T\mathbf{w}\right) = \sqrt{\gamma}\mathrm{Re}\left(s_n\right),\ \mathrm{Im}\left(\mathbf{h}_n^T\mathbf{w}\right) = \sqrt{\gamma}\mathrm{Im}\left(s_n\right). \quad (11)$$

2) Relaxed detection region characterization for $s_n \in \mathfrak{s}_4$: In another approach, the points of $s_n \in \mathfrak{s}_4$ can be considered to be placed within a square-shaped detection region. This approach is illustrated in Fig. 1(d) with gray squares. The relaxed detection region design results in a further energy-efficient transmitter, however, it increases the SER at the receiver since the minimum Euclidean distance between the received constellation points as in conventional M-QAM does not hold anymore. The related expressions to describe the relaxed detection region are

$$\begin{aligned}\sqrt{\gamma}\mathrm{Re}\left(s_n\right) - d_0 \le \mathrm{Re}\left(\mathbf{h}_n^T\mathbf{w}\right) \le \sqrt{\gamma}\mathrm{Re}\left(s_n\right) + d_0,\\ \sqrt{\gamma}\mathrm{Re}\left(s_n\right) - d_0 \le \mathrm{Im}\left(\mathbf{h}_n^T\mathbf{w}\right) \le \sqrt{\gamma}\mathrm{Im}\left(s_n\right) + d_0,\end{aligned} \quad (12)$$

where d_0 is the Euclidean distance between the edge of the relaxed detection region and the constellation point as shown in Fig. 1(d).

Choosing the proper value of d_0 depends on the target metric such as total consumed power and SER. As an approach to derive the optimal value of d_0, we can perform a 1D search over d_0 to maximize the goodput [26] over the total consumed power, which is defined as follows:

$$\eta = \frac{R\left(1 - SER\right)}{\left\|\mathbf{w}\right\|^2}, \quad (13)$$

where R is the bit per symbol, and $\left\|\mathbf{w}\right\|^2$ is the total consumed power at the transmitter. We will quantify the metric η in Section V and find its optimal value.

D. The Case of $M = 32$

The extended detection regions for $s_n \in \mathfrak{s}_5$ and $s_n \in \mathfrak{s}_6$ in the first quadrant of Fig. 1(e) are characterized as

$$3\sqrt{\gamma} \le \mathrm{Im}\left(\mathbf{h}_n^T\mathbf{w}\right) \le \mathrm{Re}\left(\mathbf{h}_n^T\mathbf{w}\right) - 2\sqrt{\gamma}, \quad (14)$$

$$\mathrm{Re}\left(\mathbf{h}_n^T\mathbf{w}\right) + 2\sqrt{\gamma} \le \mathrm{Im}\left(\mathbf{h}_n^T\mathbf{w}\right), \mathrm{Re}\left(\mathbf{h}_n^T\mathbf{w}\right) \ge 3\sqrt{\gamma}. \quad (15)$$

To model the extended detection region for $s_n \in \mathfrak{s}_5$ and $s_n \in \mathfrak{s}_6$ in the other quadrants of Fig. 1(e), we can rotate them so that they fall within $s_n \in \mathfrak{s}_5$ and $s_n \in \mathfrak{s}_6$ in the first quadrant. Then, we can use the the developed expressions for the first quadrant points in (14) and (15) to characterize the extended detection region for $s_n \in \mathfrak{s}_5$ and $s_n \in \mathfrak{s}_6$ which are are not in the first quadrant.

The extended detection regions of $s_n \in \mathfrak{s}_2$ and $s_n \in \mathfrak{s}_3$ are modeled similarly as in (7) and (10), respectively. For $s_n \in \mathfrak{s}_4$, the fixed points are modeled as (11) and the relaxed points are modeled as (12). The relaxed detection regions for $s_n \in \mathfrak{s}_4$ of 32-QAM modulation are shown in Fig. 1(f) using gray squares.

In the next section, we design the optimal symbol-level precoders for M-QAM directional modulation transmitter.

IV. Symbol-level Precoder Design for Directional Modulation

In this part, we design optimal M-QAM directional modulation precoders using the developed characterized extended and relaxed detection regions of Section III. To this end, first, we formulate optimal precoder design problems in Section IV-A aiming to minimize the transmitter power while satisfying the SNR constraints at the receiver antennas. Second, we consider minimizing the output power of the amplifier signal in each transmitter RF chain in Section IV-B while satisfying the required SNR at the receiver antennas. We refer to this as spatial peak power minimization.

A. Optimal Precoder Design: Transmit Power Minimization

In this part, we formulate and design the optimal M-QAM MIMO directional modulation precoder when the objective is to minimize the total transmission power while satisfying the required SNR at the receiving antennas.

The design problem for 4-PSK case can be written as

$$\begin{aligned}\min_{\mathbf{w}}\ & \left\|\mathbf{w}\right\|^2\\ \text{s.t. }& \mathrm{Re}\left(s_{n_1}\right)\mathrm{Re}\left(\mathbf{h}_{n_1}^T\mathbf{w}\right) \ge \sqrt{\gamma}\mathrm{Re}^2\left(s_{n_1}\right), s_{n_1} \in \mathfrak{s}_{1_4}\\ & \mathrm{Im}\left(s_{n_1}\right)\mathrm{Im}\left(\mathbf{h}_{n_1}^T\mathbf{w}\right) \ge \sqrt{\gamma}\mathrm{Im}^2\left(s_{n_1}\right).\end{aligned} \quad (16)$$

We can cast the optimal precoder design for 8-QAM modulation as

$$\begin{aligned}\min_{\mathbf{w}}\ & \left\|\mathbf{w}\right\|^2\\ \text{s.t. }& \mathrm{Re}\left(s_{n_1}\right)\mathrm{Re}\left(\mathbf{h}_{n_1}^T\mathbf{w}\right) \ge \sqrt{\gamma}\mathrm{Re}^2\left(s_{n_1}\right), s_{n_1} \in \mathfrak{s}_{1_8} && (17a)\\ & \mathrm{Im}\left(s_{n_1}\right)\mathrm{Im}\left(\mathbf{h}_{n_1}^T\mathbf{w}\right) \ge \sqrt{\gamma}\mathrm{Im}^2\left(s_{n_1}\right), && (17b)\\ & \mathrm{Re}\left(\mathbf{h}_{n_2}^T\mathbf{w}\right) = \sqrt{\gamma}\mathrm{Re}\left(s_{n_2}\right), s_{n_2} \in \mathfrak{s}_2 && (17c)\\ & \mathrm{Im}\left(s_{n_2}\right)\mathrm{Im}\left(\mathbf{h}_{n_2}\mathbf{w}\right) \ge \sqrt{\gamma}\mathrm{Im}^2\left(s_{n_2}\right). && (17d)\end{aligned}$$

Next, we can formulate the optimal precoder design problem for 16-QAM as follows

$$\begin{aligned}\min_{\mathbf{w}}\ & \left\|\mathbf{w}\right\|^2\\ \text{s.t. }& \mathrm{Re}\left(s_{n_1}\right)\mathrm{Re}\left(\mathbf{h}_{n_1}^T\mathbf{w}\right) \ge \sqrt{\gamma}\mathrm{Re}^2\left(s_{n_1}\right), s_{n_1} \in \mathfrak{s}_{1_{16}} && (18a)\\ & \mathrm{Im}\left(s_{n_1}\right)\mathrm{Im}\left(\mathbf{h}_{n_1}^T\mathbf{w}\right) \ge \sqrt{\gamma}\mathrm{Im}^2\left(s_{n_1}\right), && (18b)\\ & \mathrm{Re}\left(\mathbf{h}_{n_2}^T\mathbf{w}\right) = \sqrt{\gamma}\mathrm{Re}\left(s_{n_2}\right), s_{n_2} \in \mathfrak{s}_2 && (18c)\\ & \mathrm{Im}\left(s_{n_2}\right)\mathrm{Im}\left(\mathbf{h}_{n_2}\mathbf{w}\right) \ge \sqrt{\gamma}\mathrm{Im}^2\left(s_{n_2}\right), && (18d)\\ & \mathrm{Re}\left(s_{n_3}\right)\mathrm{Re}\left(\mathbf{h}_{n_3}^T\mathbf{w}\right) \ge \sqrt{\gamma}\mathrm{Re}^2\left(s_{n_3}\right), s_{n_3} \in \mathfrak{s}_3 && (18e)\\ & \mathrm{Im}\left(\mathbf{h}_{n_3}^T\mathbf{w}\right) = \sqrt{\gamma}\mathrm{Im}\left(s_{n_3}\right). && (18f)\\ & \mathrm{Re}\left(\mathbf{h}_{n_4}^T\mathbf{w}\right) = \sqrt{\gamma}\mathrm{Re}\left(s_{n_4}\right), s_{n_4} \in \mathfrak{s}_4 && (18g)\\ & \mathrm{Im}\left(\mathbf{h}_{n_4}^T\mathbf{w}\right) = \sqrt{\gamma}\mathrm{Im}\left(s_{n_4}\right). && (18h)\end{aligned}$$

In the case of relaxed detection region design for inner points, the constraints (18g) and (18h) are replaced by the constraints in (12). Finally, the optimal precoder design problem for 32-QAM constellation is defined as

$$\begin{aligned}
\min_{\mathbf{w}} \quad & \|\mathbf{w}\|^2 \\
\text{s.t.} \quad & \mathrm{Re}\left(\mathbf{h}_{n_2}^T\mathbf{w}\right) = \sqrt{\gamma}\mathrm{Re}\left(s_{n_2}\right),\ s_{n_2} \in \mathfrak{s}_2 && \text{(19a)}\\
& \mathrm{Im}\left(s_{n_2}\right)\mathrm{Im}\left(\mathbf{h}_{n_2}\mathbf{w}\right) \geq \sqrt{\gamma}\mathrm{Im}^2\left(s_{n_2}\right), && \text{(19b)}\\
& \mathrm{Re}\left(s_{n_3}\right)\mathrm{Re}\left(\mathbf{h}_{n_3}^T\mathbf{w}\right) \geq \sqrt{\gamma}\mathrm{Re}^2\left(s_{n_3}\right),\ s_{n_3} \in \mathfrak{s}_3 && \text{(19c)}\\
& \mathrm{Im}\left(\mathbf{h}_{n_3}^T\mathbf{w}\right) = \sqrt{\gamma}\mathrm{Im}\left(s_{n_3}\right), && \text{(19d)}\\
& \mathrm{Re}\left(\mathbf{h}_{n_4}^T\mathbf{w}\right) = \sqrt{\gamma}\mathrm{Re}\left(s_{n_4}\right),\ s_{n_4} \in \mathfrak{s}_4 && \text{(19e)}\\
& \mathrm{Im}\left(\mathbf{h}_{n_4}^T\mathbf{w}\right) = \sqrt{\gamma}\mathrm{Im}\left(s_{n_4}\right), && \text{(19f)}\\
& 3\sqrt{\gamma} \leq \mathrm{Im}\left(\widetilde{\mathbf{h}}_{n_5}^T\mathbf{w}\right) \leq \mathrm{Re}\left(\widetilde{\mathbf{h}}_{n_5}^T\mathbf{w}\right) - 2\sqrt{\gamma}, s_{n_5} \in \mathfrak{s}_5 && \text{(19g)}\\
& \mathrm{Re}\left(\widetilde{\mathbf{h}}_{n_6}^T\mathbf{w}\right) + 2\sqrt{\gamma} \leq \mathrm{Im}\left(\widetilde{\mathbf{h}}_{n_6}^T\mathbf{w}\right),\ s_{n_6} \in \mathfrak{s}_6 && \text{(19h)}\\
& \mathrm{Re}\left(\widetilde{\mathbf{h}}_{n_6}^T\mathbf{w}\right) \geq 3\sqrt{\gamma}, && \text{(19i)}
\end{aligned}$$

where $\widetilde{\mathbf{h}}_{n_5}^T = \mathbf{h}_{n_5}^T e^{i\varphi_{n_5}}$, $\widetilde{\mathbf{h}}_{n_6}^T = \mathbf{h}_{n_6}^T e^{i\varphi_{n_6}}$, φ_{n_5} is the phase difference between s_0, shown in Fig. 1(e), and $s_{n_5} \in \mathfrak{s}_5$, φ_{n_6} is the phase difference between s_{00}, shown in Fig. 1(e), and $s_{n_6} \in \mathfrak{s}_6$. In the case of relaxed design for inner constellation points, we can replace the constraints (19e) and (19f) by the constraints in (12).

Here, we proceed with transforming the 32-QAM precoder design in (19) into a standard convex form when considering fixed and relaxed detection regions for the points $s_{n_4} \in \mathfrak{s}_4$. A similar approach can be applied to the design problems in (16) to (18) in order to transform them into standard convex forms.

After applying a series of algebraic operations on (19), which are shown in Appendix A, the simplified 32-QAM design problem can be cast as

$$\begin{aligned}
\min_{\mathbf{w}} \quad & \|\mathbf{w}\|^2 \\
\text{s.t.} \quad & \mathbf{A}\mathbf{w} \geq \mathbf{a},\ \mathbf{B}\mathbf{w} = \mathbf{b}, && \text{(20)}
\end{aligned}$$

where $\mathbf{A}$, $\mathbf{a}$, $\mathbf{B}$, and $\mathbf{b}$ are defined in (31). In the case of relaxed detection region design for the points $s_{n_4} \in \mathfrak{s}_4$, we can reach a problem with the same format as in (20) where $\mathbf{A}$, $\mathbf{a}$, $\mathbf{B}$ and $\mathbf{b}$ are defied as in (32).

As we see, (20) is a convex linearly constrained quadratic programming problem and can be solved efficiently using convex optimization techniques.

B. Optimal Precoder Design: Spatial Peak Power Minimization

In this part, we design the optimal M-QAM directional modulation precoders for $M = 4, 8, 16, 32$ constellations aiming at keeping the power output of each power amplifier as low as possible. We pursuit this design while satisfying the required SNR at the receiving antennas. Note that in another approach we can minimize the transmission power while keeping the output power of each RF chain below a specific value and satisfying the required SNR at the receiving antennas.

The optimal spatial peak power minimization precoder design problem for 4-QAM modulation is written as

$$\begin{aligned}
\min_{\mathbf{w}} \quad & \max_{k=1,\ldots,N_t} \ \mathbf{w}^H\mathbf{E}_k\mathbf{w} \\
\text{s.t.} \quad & \Omega_{M-QAM}, && \text{(21)}
\end{aligned}$$

where Ω_{M-QAM} is the constellation-specific constraint set which can be found for $M = 4, 8, 16, 32$ in (16), (17), (18), and (19), respectively. In the case of relaxed detection region design for $s_{n_4} \in \mathfrak{s}_4$, the related constraints, defined in (18) and (19), are replaced by the constraints in (12).

Here, we proceed with transforming (21) for $M = 32$ into a standard form. A similar approach can be applied to the design problems for $M = 4, 8, 16$. First, we move the objective of (21) to the constraint by introducing the auxiliary variable t as

$$\begin{aligned}
\min_{\mathbf{w}} \quad & t \\
\text{s.t.} \quad & \mathbf{w}^H\mathbf{E}_k\mathbf{w} \leq t,\ \ \forall\, k = 1, ..., N_t \\
& \Omega_{M-QAM}. && \text{(22)}
\end{aligned}$$

To simplify (22) for $M = 32$, we can apply a similar process used in Appendix A for (19) to get

$$\begin{aligned}
\min_{\mathbf{w}} \quad & t \\
\text{s.t.} \quad & \mathbf{w}^T\widetilde{\mathbf{E}}_k\mathbf{w} \leq t,\ \ \forall\, k = 1, ..., N_t \\
& \mathbf{A}\mathbf{w} \geq \mathbf{a},\ \mathbf{B}\mathbf{w} = \mathbf{b}, && \text{(23)}
\end{aligned}$$

where $\mathbf{A}$, $\mathbf{a}$, $\mathbf{B}$ and $\mathbf{b}$ are as in (31). As we see, (23) is a convex problem which can be solved efficiently. If we consider the relaxed detection region design for $s_{n_4} \in \mathfrak{s}_4$, we get a similar problem as in (23) where $\mathbf{A}$, $\mathbf{a}$, $\mathbf{B}$, and $\mathbf{b}$ are the same as (32).

V. Simulation Results

In this section, we demonstrate the performance of the proposed methods and compare them with the benchmark schemes. We use average over various designed precoders to measure the performance metrics: total power consumption, maximum spatial peak power among RF chains, SER, and bit error rate (BER). Each designed precoder in the proposed method is used to communicate N_r symbols. In all simulations, channels are considered to be quasi static block Rayleigh fading generated as i.i.d. complex Gaussian random variables with distribution $\mathcal{CN}(0, 1)$ and remain fixed during the communication of a group of N_r M-QAM symbols. Also, the noise is generated using i.i.d. complex Gaussian random variables with distribution $\mathcal{CN}(0, \sigma^2)$. We assume adaptive coding and modulation in the simulation scenarios and consider specific SNR range in which each modulation order operates.

To save space, we use the acronyms "DM", "Opt LP", and "PPM" in the legend of the figures instead of the terms "directional modulation", "Optimal linear precoding" method of [27], and "spatial peak power minimization", respectively. In the following, we first mention the benchmark schemes and then proceed with the simulation scenarios.

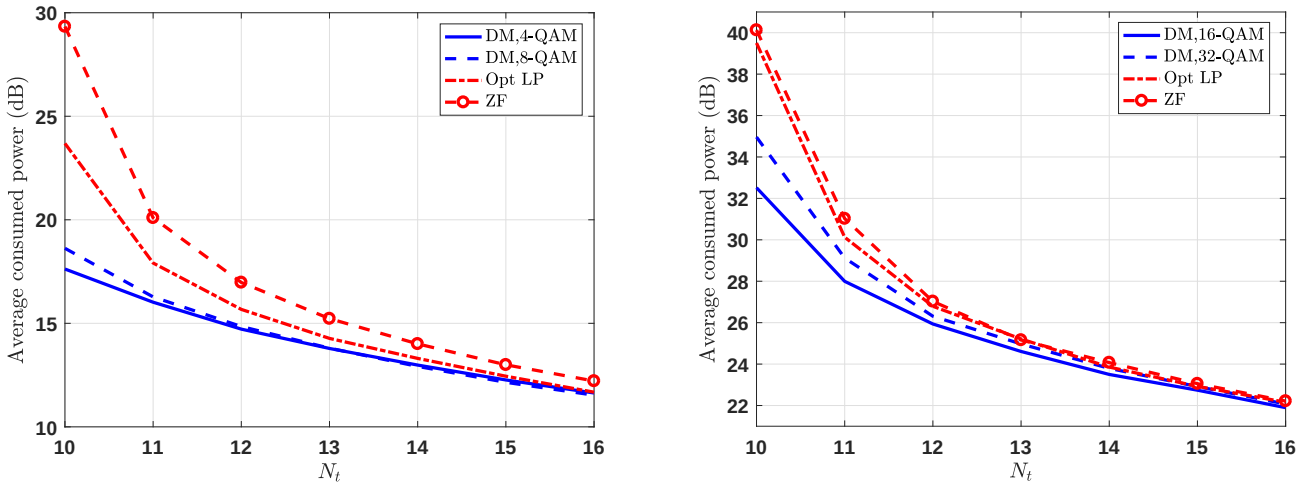

(a) $SNR = 10$ dB. (b) $SNR = 20$ dB.

Fig. 2: Average total consumed power with respect to N_t for the proposed M-QAM directional modulation precoding and the benchmark schemes when total and spatial peak power minimization designs are considered with $N_r = 10$.

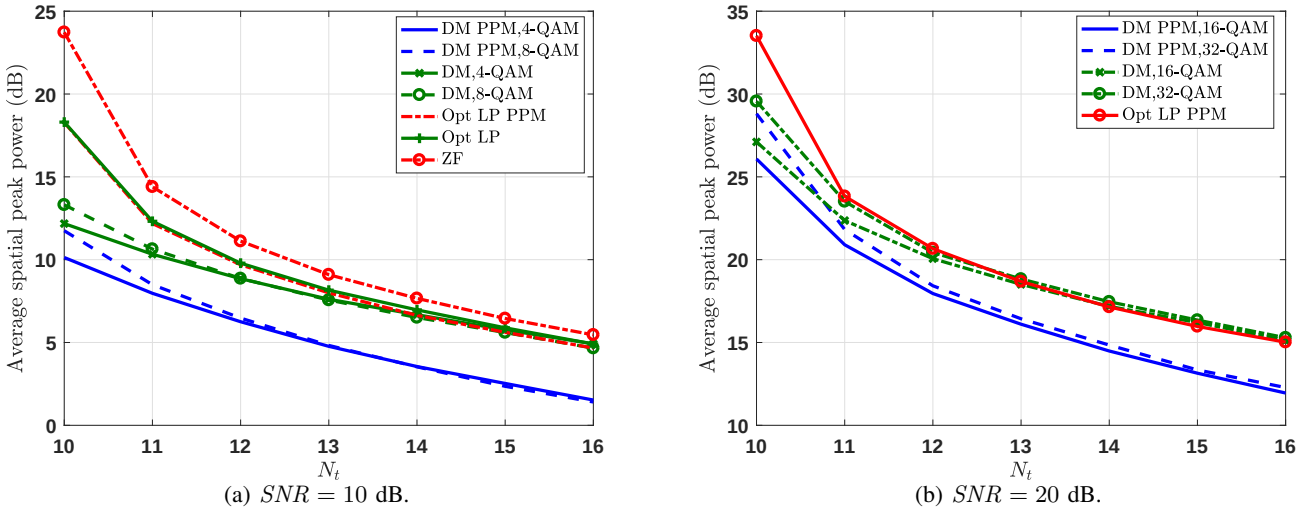

(a) $SNR = 10$ dB. (b) $SNR = 20$ dB.

Fig. 3: Average maximum peak power among the RF transmit chains with respect to N_t for the proposed M-QAM directional modulation precoding and the benchmark schemes when total and spatial peak power minimization designs are considered with $N_r = 10$.

A. Benchmark Schemes

In this part, we mention the zero-forcing [28] at the transmitter, and optimal linear precoding [27] as the comparison benchmark schemes.

1) ZF: We consider zero-forcing (ZF) at the transmitter [29] as one of the benchmark schemes since both directional modulation and ZF use the CSI knowledge at the transmitter to design the precoder and ZF results in interference-free MIMO communication. In the benchmark scheme, we apply the ZF precoder at the transmitter to remove the interference among the transmitted symbol streams. After applying ZF, the received signal at R is

$$\mathbf{y} = \mathbf{HWs} + \mathbf{n}, \tag{24}$$

where $\mathbf{W} = \mathbf{H}^H\left(\mathbf{HH}^H\right)^{-1}$ is the precoding vector and vector $\mathbf{s}$ contains the symbols to be transmitted.

2) Optimal linear precoding: The optimal linear precoding design problem using channel state information can be written as [27]

$$\min_{\mathbf{w}_1,\ldots,\mathbf{w}_{N_r}} \sum_{i=1}^{N_r} \|\mathbf{w}_i\|^2$$

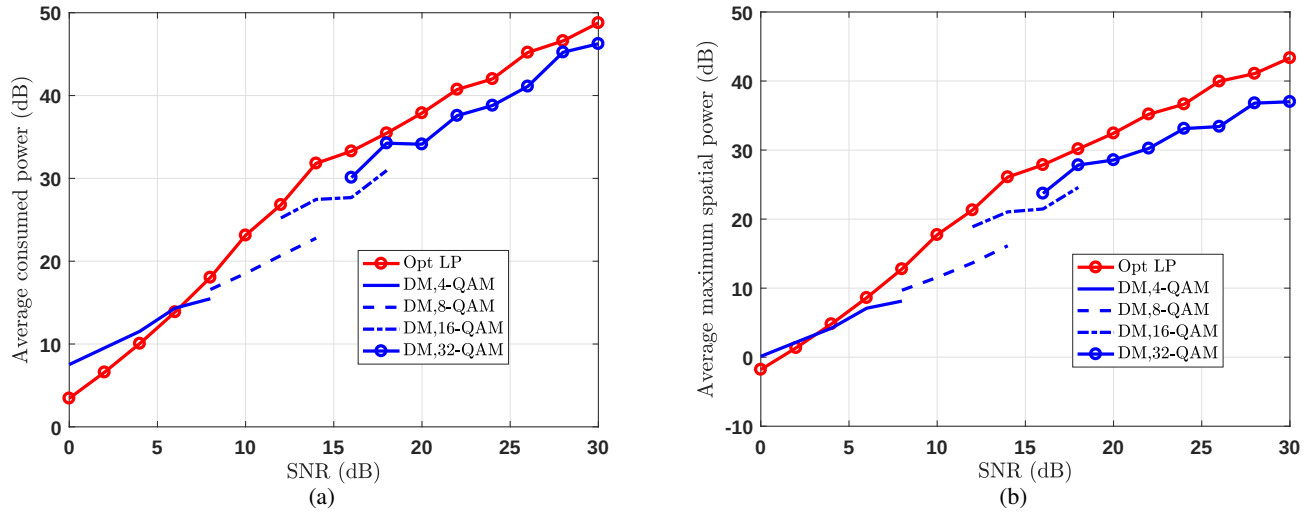

Fig. 4: Average total consumed and spatial peak powers with respect to the required SNR for the proposed M-QAM directional modulation precoding and the benchmark schemes when $N_t = N_r = 10$.

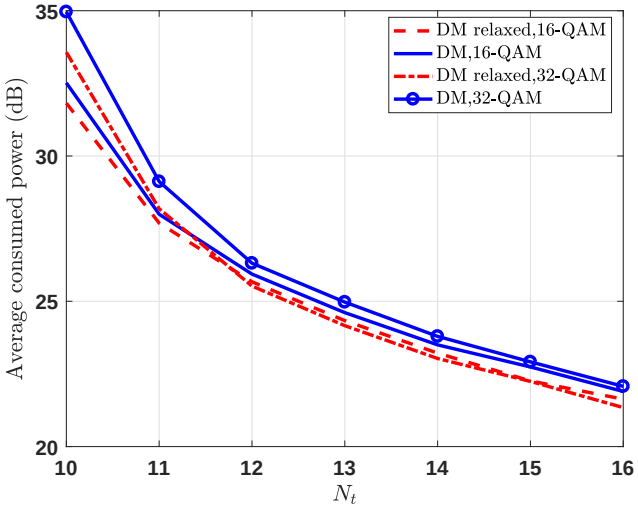

Fig. 5: Average consumed power with respect to N_t for the proposed M-QAM directional modulation precoding scheme with total power minimization when fixed and relaxed, $d_0 = 1$, detection region designs for $s_{n_4} \in \mathfrak{s}_4$ are considered with $N_r = 10$ and $SNR = 20$ dB.

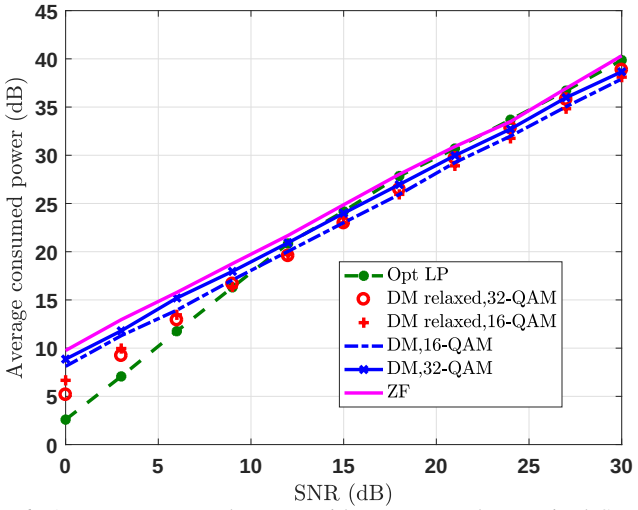

Fig. 6: Average consumed power with respect to the required SNR at the receiver for the proposed M-QAM directional modulation precoding and the benchmark schemes when $N_t = 11$, $N_r = 10$, and $d_0 = 0.4$.

$$\text{s.t.} \quad \frac{\left\|\mathbf{h}_k^T \mathbf{w}_k\right\|^2}{\sum\limits_{j \neq k}^{N_r} \mathbf{h}_j^T \mathbf{w}_j + \sigma^2} \geq \gamma, \quad \forall\, k = 1, ..., N_r. \tag{25}$$

The precoder design problem in (25) can be solved using semidefinite programming and rank-one relaxation. If the solution to (25) happens not to be rank-one, randomization can be used to derive a rank-one solution [30].

The instantaneous spatial peak power minimization version of (25), can be cast as

$$\begin{aligned} \min_{\mathbf{w}_1, ..., \mathbf{w}_{N_r}, \mathbf{t}} \quad & \|\mathbf{t}\|^2 \\ \text{s.t.} \quad & \mathbf{w}_1 \mathbf{E}_i \mathbf{w}_1 + ... + \mathbf{w}_{N_r} \mathbf{E}_i \mathbf{w}_{N_r} \leq t_i, \quad \forall\, i = 1, ..., N_t, \\ & \frac{\left\|\mathbf{h}_k^T \mathbf{w}_k\right\|^2}{\sum\limits_{j \neq k}^{N_r} \mathbf{h}_j^T \mathbf{w}_j + \sigma^2} \geq \gamma, \quad \forall\, k = 1, ..., N_r, \end{aligned} \tag{26}$$

where $\mathbf{t} = [t_1, ..., t_{N_r}]$. A similar approach as in (25) can

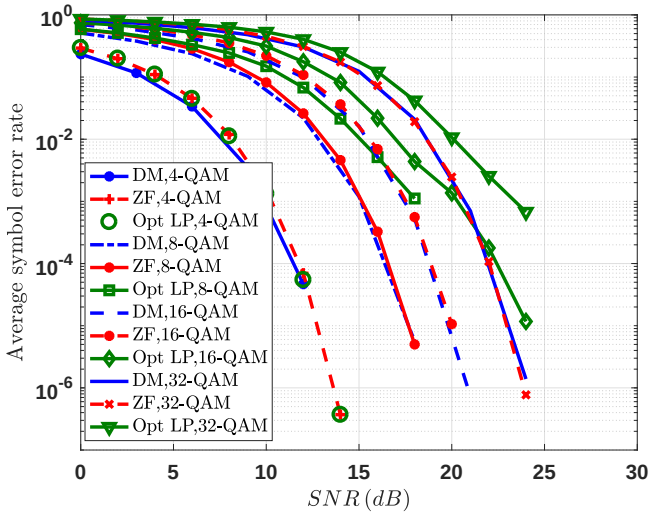

Fig. 7: Average SER with respect to the required SNR at the receiver for the proposed M-QAM directional modulation precoding and the benchmark schemes when $N_t = N_r = 10$.

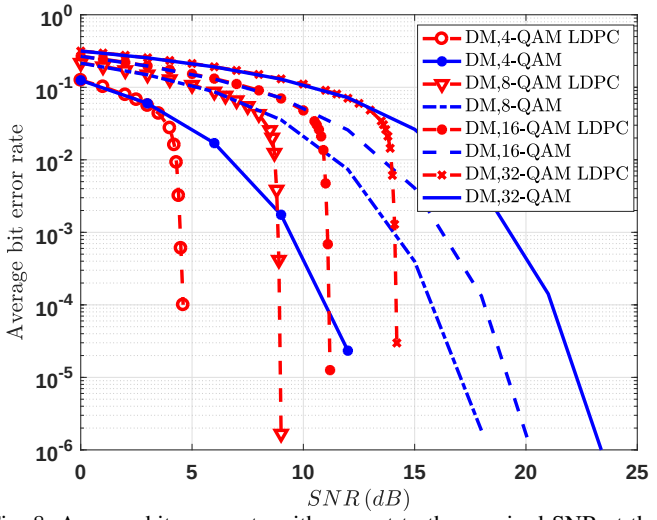

Fig. 8: Average bit error rate with respect to the required SNR at the receiver for the proposed M-QAM directional modulation precoding with and without LDPC forward error correction code when code rate is $5/6$ and $N_t = N_r = 10$.

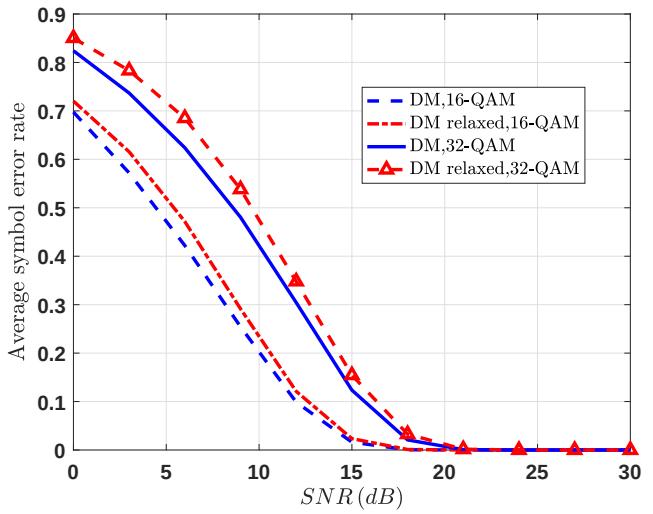

Fig. 9: Average SER with respect to the required SNR at the receiver for the proposed M-QAM directional modulation precoding when fixed and relaxed, $d_0 = 0.4$, detection region designs for $s_{n_4} \in \mathfrak{s}_4$ are considered with $N_t = N_r = 10$.

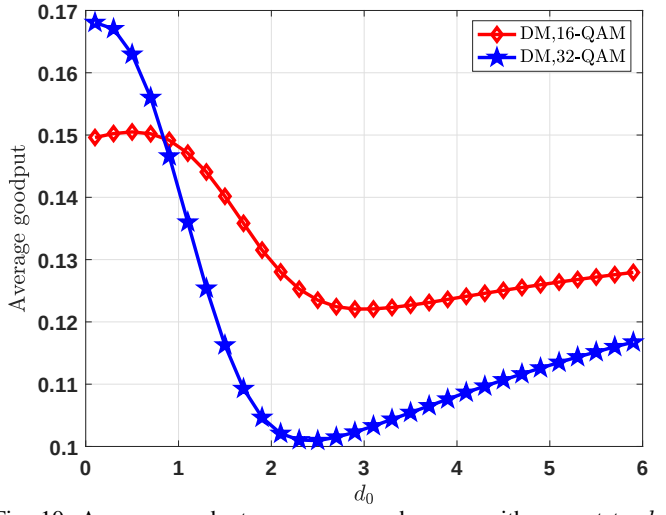

Fig. 10: Average goodput over consumed power with respect to d_0 for the proposed 16 and 32-QAM directional modulation precoding schemes when $N_t = N_r = 10$ and $SNR = 16$ dB.

be used to solve (26). The spatial peak power is minimized in (26) over the precoding vectors $\mathbf{w}_i$, however, in optimal linear precoding, the precoding vectors $\mathbf{w}_i$ will be multiplied by the M-QAM symbols, summed as $\mathbf{y}_t = \sum_{i=1}^{N_r} \mathbf{w}_i s_i$, and transmitted. As a result, this may change the transmission power of the antennas. To effectively minimize the maximum element of the transmit signal $\mathbf{y}_t$, we need to minimize each element of $\overline{\mathbf{w}} = \sum_{i=1}^{N_r} \mathbf{w}_i$ since the elements of each $\mathbf{w}_i$ are multiplied by the symbols and then summed up.

B. Simulation Scenarios

For the first scenario, we measure the transmitter's average consumed power and spatial peak power for the proposed M-QAM directional modulation as well as the benchmark schemes with respect to transmitter's number of antennas, N_t. The average total consumed power of the proposed and benchmark schemes versus N_t are shown in Fig. 2 for specific system parameters. As we see, the proposed 4, 8, 16, and 32-QAM directional modulation precoder designs with power minimization consume considerably less power than the ZF

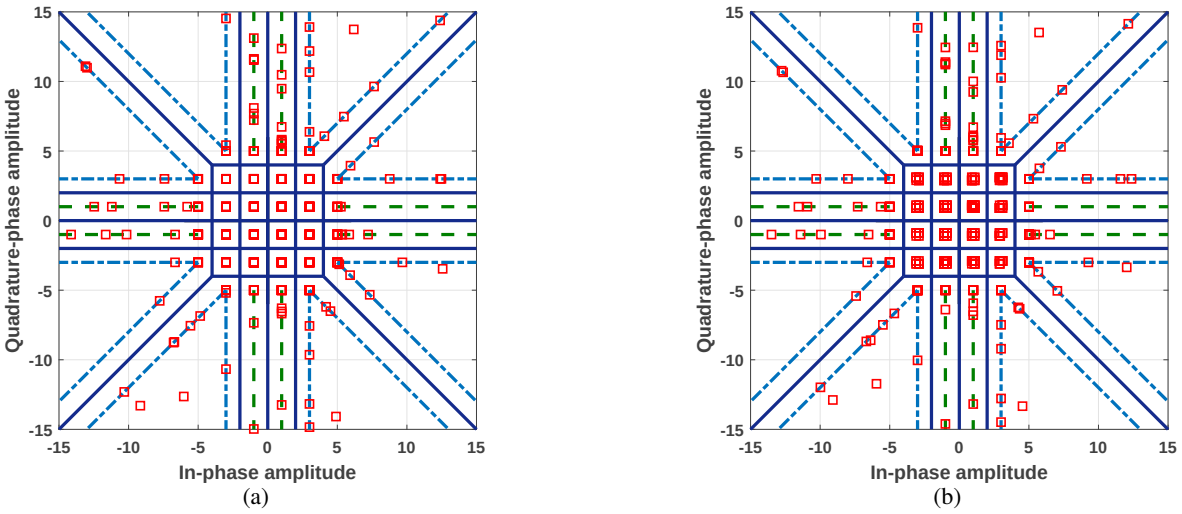

Fig. 11: The constellation of the induced symbols at the receiver for the proposed 32-QAM directional modulation precoding with $N_t = N_r = 500$ and $\gamma = 20$ when fixed detection, Fig. 11(b) and relaxed, Fig. 11(a), with $d_0 = 0.1$ region design of $s_{n_4} \in \mathfrak{s}_4$ is considered.

and optimal linear precoding schemes for specific range of N_t, especially for close values of N_t and N_r. As the modulation order decreases, the difference between the consumed power by the proposed and the benchmark schemes increases. For instance when $N_t = N_r = 10$ and $SNR = 10$ dB, 4-QAM and 8-QAM are 6.07 dB, 5.07 below the optimal linear precoding benchmark, also 16-QAM and 32-QAM are 6.98 dB and 4.54 dB below the benchmark scheme for $SNR = 20$ dB. The reason is that in contrast to the conventional ZF and optimal linear precoding, directional modulation takes advantage of the available detection regions of the M-QAM constellation by symbol-level precoding. This lets the symbols be placed in the optimal location of the defined regions while satisfying the required SNR at the receiving antennas.

The MIMO communication systems usually operate in square mode, i.e., equal number of transmit and receive antenna, since the multiplexing gain of the system is the minimum of transmit and receive antennas. Hence, the proposed scheme is a good candidate for MIMO systems since it provides the highest gain compared to optimal linear precoding for $N_t = N_r$, as Fig. 2 shows.

We investigate the spatial peak power in the second scenario. The average spatial peak power with respect to N_t is shown in Fig. 3. Average spatial peak power with respect to N_t are presented in Fig. 3. The first observation is that as the number of transmit antennas, N_t, increases, the transmitter ability to reduce the maximum output power among the power amplifiers increases. The second observation is that for lower modulation orders, the transmitter with spatial peak power minimization is more capable of reducing the level of the power amplifier signal while satisfying the SNR requirements at the receiving antennas. It is seen that the benchmark schemes result in a higher spatial peak power compared to the proposed schemes.

To analyze the effect of relaxed detection region for $s_{n_4} \in \mathfrak{s}_4$ of 16-QAM and 32-QAM constellations introduced in Section III, we have shown the average consumed power of the relaxed design with respect to N_t in Fig. 5. As it is illustrated, the relaxed detection region design for $s_{n_4} \in \mathfrak{s}_4$ results in a lower power consumption. Interestingly, as N_t increases, the average consumed power of 32-QAM gets close to that of 16-QAM in a lower N_t in the relaxed detection region design case compared to the fixed design.

In the next scenario, we measure the average consumed power, average maximum spatial peak power, and the average symbol error rate with respect to the required SNR at the receiver. The average consumed power with respect to the required SNR is shown in Fig. 4(a) for $N_t = N_r = 10$. As it is observed, the consumed power increases consistently with respect to the required SNR. In relatively middle and high SNR regimes, the proposed scheme results in a lower power consumption compared to the optimal linear precoding. The average maximum spatial peak power with respect to SNR is shown in Fig. 4(b). As it is seen, directional modulation results in a lower spatial peak power compared to the optimal linear precoding in relatively middle and high SNR regimes.

To study the effect of relaxed detection region design for $s_{n_4} \in \mathfrak{s}_4$ with respect to SNR, the average total consumed power with respect to SNR is presented in Fig. 6 for $N_t = 11$ and $N_r = 10$. The results shows that the relaxed design results in lower power consumption in low SNR regime. As SNR increases, the consumed powers by the fixed and relaxed designs converge. This is due to the fact that as the required SNR at the destination increases, the relaxed detection region gets relatively smaller compared to the required SNR and consequently the gain of relaxed design fades out. It is seen that 32-QAM with relaxed design consumes lower power than 16-QAM in low SNR since 32-QAM has four times more constellation points with relaxed design compared to 16-QAM.

The average SER with respect to the required SNR is shown in Fig. 7. It is observed that the SER of ZF is close to our scheme since it totally neutralize the interference in the extended detection region design. On the other hand, the optimal linear precoding results in a higher SER compared to the proposed schemes, especially for $M = 8, 16, 32$, since it does not fully mitigate the interference. In addition, the difference in the SER of the proposed method and optimal linear precoding goes higher as the SNR increases. The effect of low density parity check code (LDPC) on BER of the proposed scheme is shown in Fig. 8. Next, we investigate the effect of the relaxed detection region on SER. The average SER with respect to SNR is shown in Fig. 9. The relaxed detection region design increases the SER in relatively low SNR regime, however, the SER gets close to the fixed design as SNR increases.

As was shown, applying the relaxed detection region results in both power reduction and SER increment. To figure out the optimal value for relaxation, d_0, we need to consider a metric which captures both power consumption and SER. To do so, let us consider the goodput over the total consumed power, mentioned in (13), as the performance metric. The value of η with respect to d_0 is presented in Fig. 10. It is observed that there exists a value of d_0 for both 16 and 32-QAM where it is possible to setup an optimal trade-off between power consumption and SER.

At the end, we present an example of the communicated 32-QAM constellation points at the receiver for both relaxed and fixed detection region designs of $s_n \in \mathfrak{s}_4$ in Figures 11(a) and 11(b). As we see, many symbols go above the required signal level at the destination, which can results in lower SER. Particularly, we see that the optimally precoded points in the sets $\mathfrak{s}_5$ and $\mathfrak{s}_6$ are concentrated at the boundary of the extended detection regions.

VI. Conclusions

In this paper, using the concepts of extended and relaxed detection regions, we formulated the optimal directional modulation precoder design problems for 4,8,16,32-QAM constellation points with total and spatial peak power minimization, to reduce the power amplifier output in each RF chain, objectives and transformed these problems into standard convex forms. Through directional modulation precoding, symbols are placed in the optimal location of extended and relaxed detection region. In the simulation results, we showed that the suggested M-QAM directional modulation precoding consumes less power than the conventional ZF in all range of SNR, and less power than the optimal linear precoding for relatively middle and high SNR regimes. We demonstrated that this difference in power consumption increases as the modulation order decreases. Also, the results showed that directional modulation results in lower spatial peak power in all SNR ranges compared to ZF as well as lower spatial peak power compared to optimal linear precoding in middle and high SNR regimes. The results showed that the difference between the average spatial peak power of the proposed and the benchmark schemes increases as the modulation order decreases.

In addition, we saw that the interference-free communication capability of directional modulation, considering fixed design for inner constellation points of $M = 16, 32$, results in lower SER at the receiver compared to optimal linear precoding. This difference in SER increases for $M = 8, 16, 32$ as SNR increases. Considering that the proposed scheme can provide both lower power consumption and SER depending on SNR and modulation order, it can provide communication at a specific rate using a lower amount of power. In case of adaptive coding and modulation, it is possible to switch to a higher order modulation, due to lower SER, using a lower power consumption at the transmitter.

We demonstrated that precoder design using the relaxed detection region for inner constellation points of 16-QAM and 32-QAM results in lower power consumption and SER increment in a specific range of SNR, which depends on the relaxation value. It was shown than the goodput over the total power consumption can be optimized for a specific relaxation value.

Appendix A
Transformation of 32-QAM Optimal Precoder Design Problem

To simplify (19), first, we stack the constraints of (19) as

$$
\begin{aligned}
\min_{\mathbf{w}} \quad & \|\mathbf{w}\|^2 \\
\text{s.t.} \quad & \mathrm{Re}\left(\mathbf{H}_2\mathbf{w}\right) = \mathbf{s}_{re_2}, && \text{(27a)}\\
& \mathrm{Im}\left(\mathbf{S}_2\right)\mathrm{Im}\left(\mathbf{H}_2\mathbf{w}\right) \geq \mathbf{s}^{\circ 2}_{im_2}, && \text{(27b)}\\
& \mathrm{Re}\left(\mathbf{S}_3\right)\mathrm{Re}\left(\mathbf{H}_3\mathbf{w}\right) \geq \mathbf{s}^{\circ 2}_{re_3}, && \text{(27c)}\\
& \mathrm{Im}\left(\mathbf{H}_3\mathbf{w}\right) = \mathbf{s}_{im_3}, && \text{(27d)}\\
& \mathrm{Re}\left(\mathbf{H}_4\mathbf{w}\right) = \mathbf{s}_{re_4}, && \text{(27e)}\\
& \mathrm{Im}\left(\mathbf{H}_4\mathbf{w}\right) = \mathbf{s}_{im_4}, && \text{(27f)}\\
& 3 \times \mathbf{1}_5 \leq \mathrm{Im}\left(\widetilde{\mathbf{H}}_5\mathbf{w}\right) \leq \mathrm{Re}\left(\widetilde{\mathbf{H}}_5\mathbf{w}\right) - 2 \times \mathbf{1}_5, && \text{(27g)}\\
& \mathrm{Re}\left(\widetilde{\mathbf{H}}_6\mathbf{w}\right) + 2 \times \mathbf{1}_6 \leq \mathrm{Im}\left(\widetilde{\mathbf{H}}_6\mathbf{w}\right), && \text{(27h)}\\
& \mathrm{Re}\left(\widetilde{\mathbf{H}}_6\mathbf{w}\right) \geq 3 \times \mathbf{1}_6, && \text{(27i)}
\end{aligned}
$$

where $\mathbf{s}_{re_j}$ and $\mathbf{s}_{im_j}$ are the vectors that respectively stack the real and imaginary parts of the symbols $s_{n_j} \in \mathfrak{s}_\mathrm{j}$ multiplied by $\sqrt{\gamma}$, $\mathbf{1}_j$ is a $Card(\mathfrak{s}_\mathrm{j}) \times 1$ vector with elements multiplied by $\sqrt{\gamma}$, and $\mathbf{S}_j$ is a diagonal matrix with diagonal entries as $s_{n_j} \in \mathfrak{s}_\mathrm{j}$. Next, we proceed to remove the real and imaginary operators from (27). Similar as in [9], we have

$$\mathrm{Re}\left(\mathbf{H}_j\mathbf{w}\right) = \mathbf{H}_{ja}\widetilde{\mathbf{w}},\ \mathrm{Im}\left(\mathbf{H}_j\mathbf{w}\right) = \mathbf{H}_{jb}\widetilde{\mathbf{w}}, \qquad (28)$$

where $\widetilde{\mathbf{w}} = \left[\mathrm{Re}\left(\mathbf{w}^T\right), \mathrm{Im}\left(\mathbf{w}^T\right)\right]^T$, $\mathbf{H}_{ja} = [\mathrm{Re}\left(\mathbf{H}_j\right), -\mathrm{Im}\left(\mathbf{H}_j\right)]$, $\mathbf{H}_{jb} = [\mathrm{Im}\left(\mathbf{H}_j\right), \mathrm{Re}\left(\mathbf{H}_j\right)]$, and $\|\widetilde{\mathbf{w}}\|^2 = \|\mathbf{w}\|^2$. Using the results in (28), we can

reformulate (27) as

$$\begin{aligned}
\min_{\mathbf{w}} \quad & \|\mathbf{w}\|^2 \\
\text{s.t.} \quad & \mathbf{H}_{2a}\mathbf{w} = \mathbf{s}_{re_2}, && \text{(29a)}\\
& \mathrm{Im}\left(\mathbf{S}_2\right)\mathbf{H}_{2b}\mathbf{w} \geq \mathbf{s}^{\circ 2}_{im_2}, && \text{(29b)}\\
& \mathrm{Re}\left(\mathbf{S}_3\right)\mathbf{H}_{3a}\mathbf{w} \geq \mathbf{s}^{\circ 2}_{re_3}, && \text{(29c)}\\
& \mathbf{H}_{3b}\mathbf{w} = \mathbf{s}_{im_3}, && \text{(29d)}\\
& \mathbf{H}_{4a}\mathbf{w} = \mathbf{s}_{re_4}, && \text{(29e)}\\
& \mathbf{H}_{4b}\mathbf{w} = \mathbf{s}_{im_4}, && \text{(29f)}\\
& 3 \times \mathbf{1}_5 \leq \widetilde{\mathbf{H}}_{5b}\mathbf{w} \leq \widetilde{\mathbf{H}}_{5a}\mathbf{w} - 2 \times \mathbf{1}_5, && \text{(29g)}\\
& \widetilde{\mathbf{H}}_{6a}\mathbf{w} + 2 \times \mathbf{1}_6 \leq \widetilde{\mathbf{H}}_{6b}\mathbf{w},\, \widetilde{\mathbf{H}}_{6a}\mathbf{w} \geq 3 \times \mathbf{1}_6, && \text{(29h)}
\end{aligned}$$

Stacking the constraints of (29) yields

$$\begin{aligned}
\min_{\mathbf{w}} \quad & \|\mathbf{w}\|^2 \\
\text{s.t.} \quad & \mathbf{A}\mathbf{w} \geq \mathbf{a},\, \mathbf{B}\mathbf{w} = \mathbf{b}, && \text{(30)}
\end{aligned}$$

where

$$\mathbf{A} = \begin{pmatrix} \mathrm{Im}\left(\mathbf{S}_2\right)\mathbf{H}_{2b} \\ \mathrm{Re}\left(\mathbf{S}_3\right)\mathbf{H}_{3a} \\ \widetilde{\mathbf{H}}_{5a} - \widetilde{\mathbf{H}}_{5b} \\ \widetilde{\mathbf{H}}_{5b} \\ \widetilde{\mathbf{H}}_{6b} - \widetilde{\mathbf{H}}_{6a} \\ \widetilde{\mathbf{H}}_{6a} \end{pmatrix},\ \mathbf{a} = \begin{pmatrix} \mathbf{s}^{\circ 2}_{im_2} \\ \mathbf{s}^{\circ 2}_{re_3} \\ 2 \times \mathbf{1}_5 \\ 3 \times \mathbf{1}_5 \\ 2 \times \mathbf{1}_6 \\ 3 \times \mathbf{1}_6 \end{pmatrix},$$

$$\mathbf{B} = \begin{pmatrix} \mathbf{H}_{2a} \\ \mathbf{H}_{3b} \\ \mathbf{H}_{4a} \\ \mathbf{H}_{4b} \end{pmatrix},\ \mathbf{b} = \begin{pmatrix} \mathbf{s}_{re_2} \\ \mathbf{s}_{im_3} \\ \mathbf{s}_{re_4} \\ \mathbf{s}_{im_4} \end{pmatrix}. \qquad (31)$$

If we consider the relaxed detection region for the points $s_{n_4} \in \mathfrak{s}_4$, we again reach to a convex problem similar as (20) where $\mathbf{A}$, $\mathbf{a}$, $\mathbf{B}$ and $\mathbf{b}$ are as follows:

$$\mathbf{A} = \begin{pmatrix} \mathrm{Im}\left(\mathbf{S}_2\right)\mathbf{H}_{2b} \\ \mathrm{Re}\left(\mathbf{S}_3\right)\mathbf{H}_{3a} \\ \mathbf{H}_{4a} \\ \mathbf{H}_{4b} \\ -\mathbf{H}_{4a} \\ -\mathbf{H}_{4b} \\ \widetilde{\mathbf{H}}_{5a} - \widetilde{\mathbf{H}}_{5b} \\ \widetilde{\mathbf{H}}_{5b} \\ \widetilde{\mathbf{H}}_{6b} - \widetilde{\mathbf{H}}_{6a} \\ \widetilde{\mathbf{H}}_{6a} \end{pmatrix},\ \mathbf{a} = \begin{pmatrix} \mathbf{s}^{\circ 2}_{im_2} \\ \mathbf{s}^{\circ 2}_{re_3} \\ \mathbf{s}_{re_4} - \mathbf{d}_0 \\ \mathbf{s}_{im_4} - \mathbf{d}_0 \\ -\mathbf{s}_{re_4} - \mathbf{d}_0 \\ -\mathbf{s}_{im_4} - \mathbf{d}_0 \\ 2 \times \mathbf{1}_5 \\ 3 \times \mathbf{1}_5 \\ 2 \times \mathbf{1}_6 \\ 3 \times \mathbf{1}_6 \end{pmatrix},$$

$$\mathbf{B} = \begin{pmatrix} \mathbf{H}_{2a} \\ \mathbf{H}_{3b} \end{pmatrix},\ \mathbf{b} = \begin{pmatrix} \mathbf{s}_{re_2} \\ \mathbf{s}_{im_3} \end{pmatrix}, \qquad (32)$$

REFERENCES

[1] "Cisco visual networking index: Forecast and methodology, 2015-2020," Cisco Systems, Tech. Rep., 2015.

[2] S. Weinstein and P. Ebert, "Data transmission by frequency-division multiplexing using the discrete fourier transform," *IEEE Trans. Commun. Technol.*, vol. 19, no. 5, pp. 628–634, Oct. 1971.

[3] D. D. Falconer, F. Adachi, and B. Gudmundson, "Time division multiple access methods for wireless personal communications," *IEEE Commun. Mag.*, vol. 33, no. 1, pp. 50–57, Jan. 1995.

[4] Q. Spencer, A. Swindlehurst, and M. Haardt, "Zero-forcing methods for downlink spatial multiplexing in multiuser MIMO channels," *IEEE Trans. Signal Process.*, vol. 52, no. 2, pp. 461–471, Feb. 2004.

[5] N. Sidiropoulos, T. Davidson, and Z.-Q. Luo, "Transmit beamforming for physical-layer multicasting," *IEEE Trans. Signal Process.*, vol. 54, no. 6, pp. 2239–2251, Jun. 2006.

[6] A. Babakhani, D. Rutledge, and A. Hajimiri, "Transmitter architectures based on near-field direct antenna modulation," *IEEE J. Solid-State Circuits*, vol. 43, no. 12, pp. 2674–2692, Dec. 2008.

[7] M. Daly and J. Bernhard, "Directional modulation technique for phased arrays," *IEEE Trans. Antennas Propag.*, vol. 57, no. 9, pp. 2633–2640, Sep. 2009.

[8] M. Daly, E. Daly, and J. Bernhard, "Demonstration of directional modulation using a phased array," *IEEE Trans. Antennas Propag.*, vol. 58, no. 5, pp. 1545–1550, May 2010.

[9] A. Kalantari, M. Soltanalian, S. Maleki, S. Chatzinotas, and B. Ottersten, "Directional modulation via symbol-level precoding: A way to enhance security," *IEEE J. Sel. Topics Signal Process.*, vol. 10, no. 8, pp. 1478–1493, Dec. 2016.

[10] A. Kalantari, C. Tsinos, M. Soltanalian, S. Chatzinotas, W.-K. Ma, and B. Ottersten, "Low peak power MIMO directional modulatino transmitter design for relaxed phase M-PSK modulation," to be sumitted to SPAWC.

[11] A. Kalantari, C. Tsinos, M. Soltanalian, S. Chatzinotas, and B. Ottersten, "MIMO directional modulation M-QAM precoding for transceivers performance enhancement," to be submitted to SPAWC.

[12] C. Masouros and E. Alsusa, "Dynamic linear precoding for the exploitation of known interference in MIMO broadcast systems," *IEEE Trans. Wireless Commun.*, vol. 8, no. 3, pp. 1396–1404, Mar. 2009.

[13] ——, "Soft linear precoding for the downlink of DS/CDMA communication systems," *IEEE Trans. Veh. Technol.*, vol. 59, no. 1, pp. 203–215, Jan. 2010.

[14] M. Alodeh, S. Chatzinotas, and B. Ottersten, "Constructive multiuser interference in symbol level precoding for the MISO downlink channel," *IEEE Trans. Signal Process.*, vol. 63, no. 9, pp. 2239–2252, May 2015.

[15] ——, "Constructive interference through symbol level precoding for multi-level modulation," in *IEEE Global Commun. Conf. (GLOBECOM)*, CA, San Diego, Dec. 2015.

[16] A. Fehske, G. Fettweis, J. Malmodin, and G. Biczok, "The global footprint of mobile communications: The ecological and economic perspective," *IEEE Commun. Mag.*, vol. 49, no. 8, pp. 55–62, Aug. 2011.

[17] L. M. Correia, D. Zeller, O. Blume, D. Ferling, Y. Jading, I. Gdor, G. Auer, and L. V. D. Perre, "Challenges and enabling technologies for energy aware mobile radio networks," *IEEE Commun. Mag.*, vol. 48, no. 11, pp. 66–72, Nov. 2010.

[18] C. Masouros and G. Zheng, "Exploiting known interference as green signal power for downlink beamforming optimization," *IEEE Trans. Signal Process.*, vol. 63, no. 14, pp. 3628–3640, Jul. 2015.

[19] M. Alodeh, S. Chatzinotas, and B. Ottersten, "Energy-efficient symbol-level precoding in multiuser MISO based on relaxed detection region," *IEEE Trans. Wireless Commun.*, vol. 15, no. 5, pp. 3755–3767, May 2016.

[20] A. A. M. Saleh, "Frequency-independent and frequency-dependent nonlinear models of TWT amplifiers," *IEEE Trans. Wireless Commun.*, vol. 29, no. 11, pp. 1715–1720, Nov. 1981.

[21] S. K. Mohammed and E. G. Larsson, "Single-user beamforming in large-scale MISO systems with per-antenna constant-envelope constraints: The doughnut channel," *IEEE Trans. Wireless Commun.*, vol. 11, no. 11, pp. 3992–4005, Nov. 2012.

[22] J. Pan and W. K. Ma, "Constant envelope precoding for single-user large-scale MISO channels: Efficient precoding and optimal designs," *IEEE J. Sel. Topics Signal Process.*, vol. 8, no. 5, pp. 982–995, Oct. 2014.

[23] D. Spano, M. Alodeh, S. Chatzinotas, and B. Ottersten, "Per-antenna power minimization in symbol-level precoding," in *IEEE Global Commun. Conf. (GLOBECOM)*, Washington, DC, USA, Dec. 2016.

[24] Y. Wu, M. Wang, C. Xiao, Z. Ding, and X. Gao, "Linear precoding for MIMO broadcast channels with finite-alphabet constraints," *IEEE Trans. Wireless Commun.*, vol. 11, no. 8, pp. 2906–2920, Aug. 2012.

[25] The 3rd Generation Partnership Project (3GPP). LTE. http://www.3gpp.org/technologies/keywords-acronyms/98-lte.

[26] M. Alodeh, S. Chatzinotas, and B. Ottersten, "Symbol-level multiuser MISO precoding for multi-level adaptive modulation: A multicast view," 2016. [Online]. Available: http://arxiv.org/abs/1601.02788

[27] M. Bengtsson and B. Ottersten, *Handbook of Antennas in Wireless Communications*. CRC Press, 2001, ch. Optimal and suboptimal transmit beamforming, pp. 18–1–18–33.

[28] W. Yu and T. Lan, "Transmitter optimization for the multi-antenna downlink with per-antenna power constraints," *IEEE Trans. Signal Process.*, vol. 55, no. 6, pp. 2646–2660, Jun. 2007.

[29] L.-U. Choi and R. Murch, "A transmit preprocessing technique for multiuser MIMO systems using a decomposition approach," *IEEE Trans. Wireless Commun.*, vol. 3, no. 1, pp. 20–24, Jan. 2004.

[30] Z.-Q. Luo, W.-K. Ma, A. M.-C. So, Y. Ye, and S. Zhang, "Semidefinite relaxation of quadratic optimization problems," *IEEE Signal Process. Mag.*, vol. 27, no. 3, pp. 20–34, May 2010.